INL/RPT-22-69323
Revision 0

Milestone 1.2.11: H_2 Production from Surrogate Non-Native Corrosion Plumes on Aluminum 6061-T6 Fuel Cladding Surrogates

September 2022

Corey D. Pilgrim, Jacy K. Conrad, Joseph R. Wilbanks, Ryan P. Morco, James W. Jones, Timothy S. Yoder, Rebecca E. Smith, and Gregory P. Horne
Idaho National Laboratory, Center for Radiation Chemistry Research

Idaho National Laboratory

INL is a U.S. Department of Energy National Laboratory operated by Batelle Energy Alliance, LLC

INL/RPT-22-69323

Milestone 1.2.11: H_2 Production from Surrogate Non-Native Corrosion Plumes on Aluminum 6061-T6 Fuel Cladding Surrogates

Corey D. Pilgrim, Jacy K. Conrad, Joseph R. Wilbanks, Ryan P. Morco, James W. Jones, Timothy S. Yoder, Rebecca E. Smith, and Gregory P. Horne
Idaho National Laboratory, Center for Radiation Chemistry Research

September 2022

Idaho National Laboratory
Center for Radiation Chemistry Research
Idaho Falls, Idaho, 83415

http://www.inl.gov

Prepared for the
U.S. Department of Energy
Office of Environmental Management
Under DOE Idaho Operations Office
Contract DE-AC07-05ID14517

Page intentionally left blank

ABSTRACT

Thick, localized, non-native corrosion plumes have been identified on Advanced Test Reactor fuel elements, raising concern about their impact on the radiolytic formation of molecular hydrogen gas (H_2) from aluminum-clad spent nuclear fuel (ASNF) under proposed extended (> 50 years) dry storage conditions. Here, we report our findings on H_2 generation from the gamma irradiation (up to 52 MGy) of surrogate non-native corrosion plume coupons: ambient-temperature-corroded (~350 days in water) aluminum alloy 6061 (AA6061-T6) coupons in helium gas environments with ~0% added relative humidity. Additionally, we provide a comparison of proposed ASNF drying techniques— vacuum drying only, vacuum drying + 100 ºC for 4 hr, and vacuum drying + 220 ºC for 4 hr—on the yield of H_2 from these surrogate systems. The presented data indicate that similar amounts of H_2 (2-3 × 10^{-3} μmol J^{-1}) are formed from gamma-irradiated AA6061-T6 coupons corroded under different temperature regimes (i.e., ambient/350 days *vs.* 90 ºC/30 days). These findings validate current, complimentary modeling predictions based on high-temperature-corrosion irradiation data only. Further, the application of a heat-treatment procedure (100 and 220 ºC), in conjunction with vacuum drying, accelerated the rate at which a steady-state H_2 yield was attained, in comparison to vacuum only, due to the removal of H_2 precursors in the form of adsorbed waters. Interestingly, within the confidence limits of our measurements, a negligible difference in total H_2 yield was found between the two investigated heat treatment procedures.

Page intentionally left blank

ACKNOWLEDGMENTS

This work was supported by the U.S. Department of Environmental Management, Office of Technology Development, under contract DE-AC07-05ID14517.

Page intentionally left blank

CONTENTS

FIGURES

TABLES

Page intentionally left blank

ACRONYMS

AA6061	aluminum alloy 6061
Al···OH	aluminum surface bound hydroxyl group
Al···OH$^{\bullet}$	aluminum surface bound hydroxyl radical
Al···OH^{-}	aluminum surface bound hydroxide group
Al···OH_2	aluminum surface bound water
Al···O$^{\bullet}$	aluminum surface bound oxygen atom
Al···O$^{\bullet-}$	aluminum surface bound oxygen radical
ASNF	aluminum-clad spent nuclear fuel
ATR	Advanced Test Reactor
CPP	Chemical Processing Plant
CR2	Center for Radiation Chemistry Research
US-DOE	United States Department of Energy
E_{γ}	gamma photon energy
EMTD	Environmental Management-Technology Development
GC	gas chromatography
Gy min^{-1}	Grays per minute
h^{+}	electron vacancy hole
H_{aq}^{+}	hydrated proton
H$^{\bullet}$	hydrogen atom
H_2	molecular hydrogen
He	helium
INL	Idaho National Laboratory
MeV	mega electron volts
MGy	mega Gray
MΩ·cm	megaohm centimeter
µm	micrometers
RH	relative humidity
TCD	thermal conductivity detector
$\tau_{1/2}$	half-life
°C	degrees Celsius
µL	microliter
µmol kg^{-1}	micromoles per kilogram

Page intentionally left blank

Milestone 1.2.11: H2 Production from Surrogate "Non-Native" Corrosion Plumes on Aluminum 6061-T6 Fuel Cladding Surrogates

1. INTRODUCTION

There are approximately 18 metric tons of aluminum-clad spent nuclear fuel (ASNF) managed by the United States Department of Energy (US-DOE) [1]. This material is currently being considered for extended (> 50 years) dry storage using the standard US-DOE canister [2-6]. To ensure a smooth transition and the continued safe storage of ASNF, the US-DOE Office of Environmental Management-Technology Development (EMTD) initiated a program to evaluate the technical basis for the extended dry storage of ASNF [2,3,7]. One of the objectives of this program is to determine the impact of ionizing radiation effects on the long-term integrity of the standard US-DOE canister, specifically molecular hydrogen (H_2) generation from the irradiation of hydrated corrosion layers on ASNF [8-11]:

$$Al\cdots OH \rightsquigarrow h^+ + Al\cdots OH^-, \quad (1)$$

$$Al\cdots OH^- \rightarrow Al\cdots O^{\bullet -} + H^\bullet, \quad (2)$$

$$Al\cdots OH_2 + h^+ \rightarrow Al\cdots OH^- + H_{aq}^+, \quad (3)$$

$$H^\bullet + Al\cdots OH_2 \rightarrow H_2 + Al\cdots OH^\bullet, \quad (4)$$

$$H^\bullet + Al\cdots OH \rightarrow H_2 + Al\cdots O^\bullet, \quad (5)$$

$$H^\bullet + H^\bullet \rightarrow H_2. \quad (6)$$

The H_2 generated in this way could lead to aluminum alloy embrittlement, canister pressurization, and the formation of explosive and/or flammable gas mixtures [12-15].

To date, this program's irradiation studies have focused on the radiolytic formation of H_2 from corroded surrogate aluminum alloy coupons, specifically 1100 and 6061, under a variety of conditions, including temperature, backfill gas composition, and relative humidity (RH) [16-23]. In these studies, corrosion was achieved by submerging the aluminum coupons in high purity water (18.2 MΩ·cm) at ~95 °C for 30 days, as benchmarked by Lister [24]. This procedure generated ~5 μm thick, heterogenous corrosion layers, with large contributions from gibbsite ($Al(OH)_3$) and boehmite (γ-AlOOH) mineral phases [16,23]. The data gathered through the irradiation of these high-temperature-corroded aluminum coupons have been essential for the development of predictive computer models to support the technical basis for the extended dry storage of ASNF in the standard US-DOE canister [25-28].

However, concern has been raised about the impact of non-native corrosion plumes on the currently established radiation chemistry of these aluminum systems and their complementary model predictions. During in-cell inspection of Advanced Test Reactor (ATR) fuel elements, Winston *et al.* found visual evidence for non-native corrosion plumes [29], an example of which is shown in Figure 1. These plumes are believed to arise from post-reactor operation damage of the initial passivated corrosion layer (i.e., the product of high-temperature-corrosion processes). Once damaged, subsequent water-

Figure 1. A closeup view of an INL ATR fuel element showing large, localized non-native corrosion plumes (highlighted by white rings) caused by a friction-type handling tool. Reproduced from reference 29.

mediated ambient-temperature-corrosion processes occurred in the ATR canal and Chemical Processing Plant (CPP)-603 basin but ceased once removed into interim dry storage [29]. Compared with the initial passivated corrosion layer (2–6 μm), the non-native corrosion plumes were found to be thicker (> 6 μm), which may translate as a greater inventory of H_2 precursors, such as a larger capacity of adsorbed water. Consequently, these plumes could contribute to a higher steady-state yield of H_2 than currently predicted.

Although samples of the non-native corrosion plumes were not collected for characterization [29], given the temperature dependence of aluminum corrosion processes [30], the mineral phase composition of these plumes is expected to be different from the initial passivated corrosion layer and the high-temperature-corrosion layers investigated by our team [16-23]. Differences in corrosion layer composition will impact the extent of H_2 production from these plumes, as demonstrated by the differences in H_2 generation found for irradiated gibbsite and boehmite powders [31-35].

Overall, understanding the radiolytic behavior of non-native corrosion plumes is essential for evaluating the H_2 production potential of real-world ASNF under envisioned extended dry storage conditions. To this end, we report our findings on H_2 generation from the irradiation (up to 52 MGy) of ambient-temperature-corroded AA6061-T6 coupons in helium gas (He) environments with ~0% added RH, as measured by gas chromatography (GC). In addition, we provide a comparison of proposed ASNF drying techniques [36-38]—for the reduction of bulk and adsorbed (physi- and chemisorbed) waters—on the steady-state yield of H_2 from these surrogate non-native corrosion plume systems.

2. EXPERIMENTAL METHODS

2.1 Materials

AA6061-T6 plates (3.15 in. × 12 in. × 0.050 in., with six ¼ in. diameter holes for mounting) were sourced from QLab Corporation (Westlake, Ohio, USA) in the as-milled surface condition. Acetone (HPLC Plus, ≥ 99.9%) and ethanol (absolute, ≥ 99.8%) were supplied by MilliporeSigma. Helium was purchased in its highest available purity from Norco. Ultra-pure water (18.2 MΩ·cm) was generated in-house using a Thermo Scientific (Waltham, MA, USA) Harvey™ DI+ Cartridge System, and used for all water applications.

2.2 Sample Preparation

The as-received AA6061-T6 plates were polished to a 600 grit finish using a handheld orbital sander, and then cleaned by rinsing sequentially with acetone, ethanol, and then water, prior to air drying. The mass, length, width, and nominal thickness was measured for each plate [37]. The plates were then mounted on a nylon holding rack with nylon spacers in between each plate to prevent them from touching one another, as shown in Figure 2. The plate corrosion assembly was then immersed in water from November 17th 2020 to November 2nd 2021 (~350 days), under ambient temperature (nominally 20 °C) conditions, to grow a thick layer of hydrated (oxy)hydroxide. During this corrosion period, the water was not changed, although the tanks were topped up to maintain a constant water level. Although surface characterization was not performed by this study, previous work using the same methodology reported the formation of 3–10 μm thick corrosion layers of predominantly bayerite mineral phases [37], which are assumed to be present on the plate recovered for this work. Post corrosion, a single AA6061-T6 plate was recovered, air dried, and then cut into smaller coupons. The mass, length, width, and surface area of each coupon was recorded prior to a given drying treatment and subsequent irradiation, as

Figure 2. Plate corrosion assembly prior to immersion.

shown in Table 1–Table 3 for vacuum drying only, vacuum drying + 100 ºC for 4 hr, and vacuum drying + 220 ºC for 4 hr treatments, respectively. The procedures for the drying processes were as follows:

- *Vacuum drying only*, AA6061-T6 coupons were loaded into a VWR (Radnor, Pennsylvania, USA) vacuum oven, and then held at ≤ 22.5 in. Hg overnight.
- *Vacuum drying + 100 ºC for 4 hr*, AA6061-T6 coupons were loaded into the same vacuum oven, which was allowed to ramp to 100 ºC under ≤ 22.5 in. Hg vacuum before leaving the coupons for 4 hours at temperature. Once the heat treatment was complete, the oven and its contents were left to cool overnight under vacuum.
- *Vacuum drying + 220 ºC for 4 hr*, AA6061-T6 coupons were loaded into the same vacuum oven, which was allowed to ramp to 220 ºC under≤22.5 in. Hg vacuum before leaving the coupons for 4 hours at temperature. Once the heat treatment was complete, the oven and its contents were left to cool over the weekend under vacuum.

Post drying, the coupons were then individually flame-sealed in borosilicate ampules backfilled with He with ~0% added RH. These sample conditions provided a direct comparison with previous irradiation data measured for AA6061-T6 coupons corroded under high-temperature conditions [22,23]. Each flame-sealed ampule was then etched with a Roman numeral for sample identity records.

Table 1. Summary of AA6061-T6 coupon masses, lengths, widths, and surface area prior to vacuum drying only treatment and irradiation.

AA6061-T6 Coupon	**Mass** (g)	**Length** (in.)	**Width** (in.)
1	0.55006	1.0240	0.2525
2	0.55610	1.0435	0.2440
3	0.52939	1.0140	0.2430
4	0.53109	1.0020	0.2470
5	0.55622	1.0255	0.2480
6	0.53166	0.9805	0.2480
7	0.54166	1.0395	0.2405
8	0.53715	1.0000	0.2465
9	0.53972	1.0345	0.2425
10	0.53126	1.0010	0.2430
11	0.54808	1.0065	0.2485
12	0.51469	0.9890	0.2390
13	0.53135	0.9990	0.2430
14	0.55453	1.0405	0.2440
15	0.53480	1.0235	0.2435
16	0.54085	1.0320	0.2395
17	0.53923	1.0155	0.2465
18	0.54935	1.0135	0.2475

Table 2. Summary of AA6061-T6 coupon masses, lengths, widths, and surface area prior to vacuum drying + 100 ºC for 4 hr treatment and irradiation.

AA6061-T6 Coupon	**Mass** (g)	**Length** (in.)	**Width** (in.)
19	0.56353	1.0355	0.2530
20	0.55471	1.0245	0.2480
22	0.54494	1.0260	0.2430
23	0.51402	0.9790	0.2435
24	0.53640	1.0080	0.2435
25	0.55048	1.0135	0.2505
26	0.55483	1.0255	0.2495
27	0.53803	1.0095	0.2460
28	0.51409	0.9870	0.2390
29	0.52729	1.0040	0.2525
31	0.53566	1.0075	0.2430
32	0.52221	0.9995	0.2410
33	0.54660	1.0085	0.2470
34	0.54600	1.0270	0.2455
35	0.54137	1.0335	0.2405
36	0.53174	0.9790	0.2485
37	0.53091	1.0020	0.2435
38	0.52393	1.0040	0.2385

Table 3. Summary of AA6061-T6 coupon masses, lengths, widths, and surface area prior to vacuum drying + 220 °C for 4 hr treatment and irradiation.

AA6061-T6 Coupon	**Mass** (g)	**Length** (in.)	**Width** (in.)
39	0.53667	1.009	0.2430
40	0.56531	1.040	0.2510
41	0.53994	1.0145	0.2475
42	0.54483	1.0265	0.2430
43	0.54549	1.0080	0.2470
44	0.52937	0.9795	0.2470
45	0.53469	1.0035	0.2425
46	0.54454	1.0020	0.2485
47	0.53475	1.0045	0.2420
48	0.52463	1.0035	0.2410
50	0.53121	1.0155	0.2410
51	0.54426	1.0055	0.2480
52	0.53782	0.9990	0.2455
53	0.53055	1.0140	0.2390
55	0.53607	1.0080	0.2475
56	0.57134	1.0355	0.2525
57	0.55796	1.0470	0.2425
58	0.53225	1.0010	0.2460

2.3 Steady-State Gamma Irradiations

Irradiations were performed using the Idaho National Laboratory (INL) Center for Radiation Chemistry Research (CR2) Foss Therapy Services (Pacoima, California, USA) Cobalt-60 gamma irradiator. Flame-sealed ampules were loaded in triplicate into a multi-position sample holder and irradiated over ~250 days under ambient irradiator temperature conditions (~45 °C, as determined using a calibrated NI USB-TC01 Single Channel Temperature Input Device equipped with a K-type thermocouple). Fricke dosimetry was used to determine the dose rate (65-456 Gy min^{-1}) at each occupied sample position in the irradiator [39]. Measured dose rates were then corrected for the decay of the cobalt-60 sources ($\tau_{1/2}$ = 5.27 years; $E_{\gamma 1}$ = 1.17 MeV and $E_{\gamma 2}$ = 1.33 MeV) and for the electron density of aluminum metal *vs.* water (0.8673) [40]. The corrected dose rates were then multiplied through by the duration of sample exposure to get the final absorbed gamma dose range, 0–53 MGy.

2.4 Gas Phase H_2 Analysis

Quantification of H_2 in the gas phase was achieved by GC using a Shimadzu Co. (Kyoto, Japan) Nexus GC-2030 gas chromatograph equipped with a thermal conductivity detector (TCD). GC settings and sampling technique were as previously described [17]. This method has an estimated error of ≤ 10% and

limits of detection of 0.01–1% H_2 at the 95% confidence level. Quality control checks were performed daily to confirm known concentrations of H_2 relative to measured calibration curves.

3. RESULTS AND DISCUSSION

The radiolytic formation of H_2 is shown in Figure 3 for the gamma irradiation of ambient-temperature-corroded AA6061-T6 coupons in He environments with ~0% added RH for each drying treatment. Plotted alongside our new data are previously reported H_2 yields (μmol kg^{-1}) from the irradiation of high-temperature-corroded, air-dried AA6061-T6 coupons [22]. For all three drying treatment procedures used in this study, the yield of H_2 increased with absorbed gamma dose, while the rate of H_2 formation (μmol J^{-1}, the *G*-value) exponentially decreased toward a steady-state yield. For the heat-treated samples, a steady-state H_2 yield appeared to be attained by 53 MGy, as indicated by the plateauing of the exponential fits in Figure 3, which correspond to: $(1.60 \pm 0.07) \times 10^{-3}$ μmol kg^{-1} for vacuum drying + 100 °C heating for 4 hrs, and $(2.13 \pm 0.05) \times 10^{-3}$ μmol kg^{-1} for vacuum drying + 220 °C heating for 4 hrs. On the other hand, the vacuum drying only samples require additional dose to reach steady-state, as indicated by the continual increase in the associated exponential fit, attaining a H_2 yield of $(2.17 \pm 0.02) \times 10^{-3}$ μmol kg^{-1} within the 53 MGy dose range of this study. All steady-state or final dose range H_2 yields are summarized in Table 4.

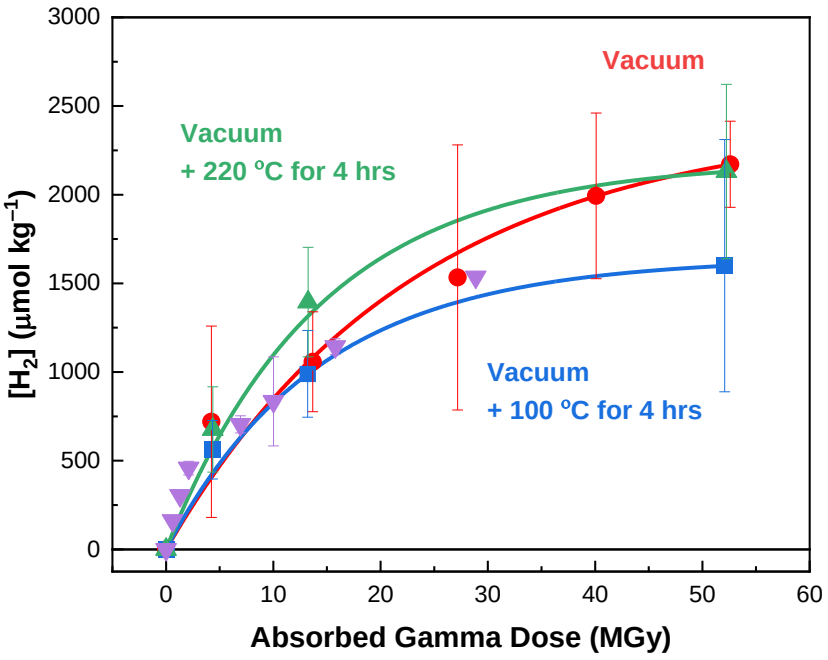

Figure 3. Concentration of H_2 (μmol kg^{-1}) as a function of absorbed gamma dose from the irradiation of corroded AA6061-T6 coupons in He environments with ~0% added RH at ambient irradiator temperature (~45 °C) for each drying condition: vacuum drying only (●); vacuum drying + 100 °C heating for 4 hrs (■); and vacuum drying + 220 °C heating for 4 hrs (▲). Solid curves are exponential fits to data to guide the eye. In addition, previously reported high-temperature-corroded, air-dried AA6061-T6 coupon data (▼) have been included for comparison [22].

It is evident from **Figure 3** that the vacuum only data are in very good agreement with its high-temperature-corroded, air-dried analogue [22], which indicates that air drying is sufficient to remove any residual bulk water contribution to radiolytic H_2 production from the irradiation of AA6061-T6 coupons. This observation also suggests that similar amounts of H_2 ($2–3 \times 10^{-3}$ μmol J^{-1}, from data extrapolation) are produced from the corrosion layers of the surrogate non-native corrosion plume samples and those

formed by high-temperature-corrosion processes. These findings further validate current modeling predictions based on high-temperature-corrosion irradiation data only [25-28], and alleviate some of the radiolytic concerns surrounding non-native corrosion plumes. However, post-irradiation surface characterization is necessary to validate these observations more conclusively.

Table 4. Comparison of steady-state or final dose range* H_2 yields from the gamma irradiation of ambient-temperature-corroded AA6061-T6 coupons in He environments with ~0% added RH for different drying treatment procedures.

Drying Treatment	**Steady-State H_2 Yield** (10^{-3} μmol J^{-1})
vacuum drying only	2.17 ± 0.24*
vacuum drying + 100 °C for 4 hours	1.60 ± 0.71
vacuum drying + 220 °C for 4 hours	2.13 ± 0.49

Concerning the impact of heat treatment procedure on the yields of H_2 shown in Figure 3 and Table 4, at first glance, the use of different heating regimes led to different radiolytic H_2 production rates, as indicated by the dissimilar steady-state yields for 100 and 220 °C treatments (Figure 3, Table 4). This expectation has been previously explained by the gradual removal of physi- and then chemisorbed waters from the coupon surface in going from 100–220 °C [36], thereby progressively inhibiting reactions 3 and 4.

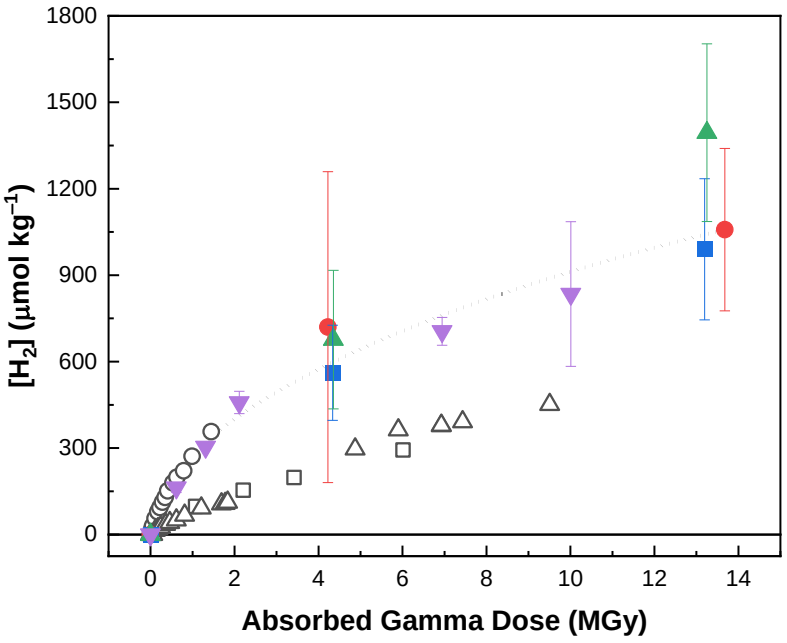

Figure 4. Comparison of H_2 yields (μmol kg^{-1}) as a function of absorbed gamma dose from the irradiation of corroded AA6061 coupons in He environments with ~0% added RH: ambient-temperature-corroded vacuum drying only (●); ambient-temperature-corroded vacuum drying + 100 °C heating for 4 hrs (■); ambient-temperature-corroded vacuum drying + 220 °C heating for 4 hrs (▲); high-temperature-corroded and air-dried (▼) [22]; As-Corroded (○) [36]; 150 °C As-Dried (□) [38]; and 220 °C As-Dried (△) [36].

However, if this were the case, we would expect there to be a lower H_2 yield for the vacuum drying + 220 °C heating for 4 hrs treatment *vs.* the vacuum drying + 100 °C heating for 4 hrs treatment, as more H_2 precursors would be removed at 220 °C. That said, the removal of chemisorbed water is not the only effect promoted at 220 °C, as we have previously shown a significant increase in H_2 formation from AA1100

coupons irradiated at 200 ºC [17]. This observation was attributed to a combination of: *(i)* the dehydration of bayerite to pseudo-boehmite, and ultimately boehmite, begins at ~170 °C [41,42]; and *(ii)* more efficient release of $H^{\bullet}$ atoms and H_2 through annealing [33,34]. Here, the vacuum drying + 220 ºC heating for 4 hrs pretreatment is expected to only influence the phase transformation of bayerite—which we assume to be the prime constituent of our ambient-temperature-corroded AA6061-T6 coupons [37]—to boehmite, which was found to be the case by Verst *et al.* [36]. The boehmite mineral phase has been shown to yield significantly more H_2 than $Al(OH)_3$ mineral phases, specifically gibbsite, attributed to the relative ease of diffusion of $H^{\bullet}$ atoms and H_2 in the boehmite lattice [31-35]. Consequently, the higher steady-state H_2 yield measured for samples from vacuum drying + 220 ºC heating for 4 hrs, as compared to vacuum drying + 100 ºC heating for 4 hrs, may be the unintentional result of temperature driven bayerite conversion to boehmite. That said, considering the confidence limits of the data measured by this work—as indicated by the error bars (1σ) in Figure 3—we find that there is negligible difference between the two investigated heat treatment procedures. This conclusion agrees with a more recent study on the relative impacts of ASNF drying treatments on the rate of H_2 generation [38], the data for which are reproduced in Figure 4 with 0-15 MGy data from Figure 3. Verst *et al.* found negligible difference in the yield of H_2 from irradiated (up to 10 MGy) AA6061-T6 plates that had received 150 or 220 ºC pretreatment and subsequent vacuum drying, the 150 ºC As-Dried and 220 ºC As-Dried data in Figure 4, respectively. The As-Corroded data in Figure 4 are for equivalent corrosion, He backfill, and added RH conditions as the vacuum drying only samples in this work and our previously reported high-temperature-corroded, air-dried samples [22], all of which are in good agreement. This observation suggests that the fabrication process for converting ambient-temperature-corroded AA6061-T6 plates into coupons does not significantly alter the corrosion layers, with respect to the potential for radiolytic H_2 generation. However, that is where the similarities between the findings of the two studies ends, as both heat treatment procedures reported by Verst *et al.* yielded significantly lower amounts of H_2 than the corresponding As-Corroded samples [38]. These findings are contrary to previous measurements for AA1100 at 200 ºC [22], the precedence for boehmite to yield more H_2 than bayerite [31-35], and the new ambient-temperature-corrosion data presented here. The source of this discrepancy is currently unknown. However, for the purposes of refining current modeling efforts, the data presented in Figures 3 and 4 provide bounding limits for H_2 production and the attainment of a steady-state yield.

4. CONCLUSIONS

The purpose of this investigation was to determine whether the steady-state yield of H_2, from the irradiation of corroded aluminum coupons, is affected by the presence of non-native corrosion plumes arising from ambient-temperature-corrosion processes. The presented data indicates that similar amounts of H_2 ($2–3 \times 10^{-3}$ μmol J^{-1}, from data extrapolation) are formed from gamma-irradiated AA6061 coupons corroded under different temperature regimes (i.e., ambient/~350 days *vs.* 90 ºC/30 days). These findings further validate current modeling predictions based on high-temperature-corrosion irradiation data only [25-28].

Additionally, this study also evaluated the impact of different proposed ASNF drying treatments—vacuum drying only, vacuum drying + 100 ºC for 4 hr, and vacuum drying + 220 ºC for 4 hr—on the yield of H_2 from these systems. Application of a heat-treatment procedure (100 and 220 ºC), in conjunction with vacuum drying, accelerated the rate at which a steady-state H_2 yield was attained, due to the removal of H_2 precursors in the form of adsorbed waters. Interestingly, within the confidence limits of our measurements, negligible difference in total H_2 yield was found between the two investigated heat-treatment procedures. However, contrary to other studies, we did not find that the application of a heat-treatment procedure significantly reduced the total yield of H_2 within the investigated dose range.

5. ACKNOWLEDGMENTS

This work was supported by the U.S. Department of Environmental Management, Office of Technology Development, under contract DE-AC07-05ID14517.

6. REFERENCES

(1) The Department of Energy Spent Fuel Database (SFD), Version 8.0.7, **2021**.

(2) M.D. Argyle, Aluminum Clad Spent Nuclear Fuel: Technical Considerations and Challenges for Extended (>50 Years) Dry Storage, *DOE/ID RPT 1575*, **2017**.

(3) M.J. Connolly, Aluminum Clad Spent Nuclear Fuel Long Term Dry Storage Technical Issues Action Plan – Technical and Engineering Activities, *INL/EXT-17-43908*, **2017**.

(4) United States Department of Energy, Preliminary Design, Specification for Department of Energy Standardized Spent Nuclear Fuel Canisters. Idaho Falls, Vol I Design Specification, **1998a**.

(5) United States Department of Energy, Preliminary Design, Specification for Department of Energy Standardized Spent Nuclear Fuel Canisters. Idaho Falls, Vol II Rationale document, **1998b**.

(6) ECAR 4632, Spencer Snow, Supplemental Evaluation of the DOE Standard SNF Canister for Accidental Drops, **2019**.

(7) E. Eidelpes, J. Jarrell, G.P. Horne, J.K. Conrad, C.D. Pilgrim, A.W. Abboud, P. L. Winston, and R. Sindelar, Technical Basis for Extended Dry Storage of Aluminum-clad Spent Nuclear Fuel. *Journal of Nuclear Materials*, **2022**, submitted.

(8) G.V. Buxton, C.L. Greenstock, W.P. Helman, and A.B. Ross, Critical review of rate constants for reactions of hydrated electrons, hydrogen atoms and hydroxyl radicals ($^{\bullet}OH/^{\bullet}O^{-}$) in aqueous solution. *J. Phys. Chem. Ref. Data*, **1988**, *17*, 513.

(9) B.H. Milosavljevic and J.K. Thomas, Reactions of Electrons on the Surface of γ-Al_2O_3. A Pulse Radiolytic Study with 0.4 MeV Electrons. *J. Phys, Chem. B*, **2003**, *107*, 11907.

(10) J.K. Thomas, Physical Aspects of Radiation-Induced Processes on SiO_2, γ-Al_2O_3, Zeolites, and Clays. *Chem. Rev.*, **2005**, *105*, 1683.

(11) S. Le Caer, Water Radiolysis: Influence of Oxide Surfaces on H_2 Production under Ionizing Radiation. *Water*, **2011**, *3*, 235.

(12) R. Ambat and E.S. Dwaarakadasa, Effect of hydrogen in aluminium and aluminium alloys: a review. *Bull. Mater. Sci.*, **1996**, *19*, 103.

(13) R.P. Gangloff and B.P. Somerday, Gaseous Hydrogen Embrittlement of Materials. In Energy Technologies, Volume 1 – the Problem, its Characterization and Effects on Particular Alloy Classes. Eds., Elsevier, New York, USA, **2012**.

(14) G. Lu and E. Kaxiras, Hydrogen embrittlement of aluminum: the crucial role of vacancies. *Phys. Rev. Lett.*, **2005**, *94*, 155501.

(15) B. Bonin, M. Colin, and A. Dutfoy, Pressure building during the early states of gas production in a radioactive waste repository. *J. Nucl. Mater.*, **2000**, *281*, 1.

(16) Elizabeth H. Parker-Quaife, Gregory P. Horne, Colt R. Heathman, Peter R. Zalupski, Radiation-Induced Changes in Corrosion of AA1100. *INL/EXT-19-52738*, **2019**.

(17) E.H. Parker-Quaife, C. Verst, C.R. Heathman, P.Z. Zalupski, and G.P. Horne, Radiation-Induced Molecular Hydrogen Gas Generation in the Presence of Aluminum Alloy 1100. *Rad. Phys. Chem.*, **2020**, *177*, 109117.

(18) G.P. Horne, E.H. Parker-Quaife, C.G. Verst, C.L. Crawford, and R.L. Sindelar, Milestone 2.6: Complete Round-Robin Hydrogen Gas Analysis Capability Comparison. *INL/EXT-20-00810*, **2020**.

(19) G.P. Horne and E.H. Parker-Quaife, Milestone 2.7: Evaluation of Techniques for the Measurement of Molecular Hydrogen Gas in Helium Matrices. *INL/EXT-20-60008*, **2020**.

(20) E.H. Parker-Quaife and G.P Horne, Milestone 2.8: Preliminary Radiolytic Gas Generation Measurements from Helium-Backfilled Samples. *INL/EXT-21-61404*, **2020**.

(21) G.P. Horne, J.K. Conrad, T.M. Copeland-Johnson, A. Khanolkar, C.D. Pilgrim, J.R. Wilbanks, C. Rae, and E.H. Parker-Quaife, Milestone 1.2.9: Radiolytic Gas Generation Measurements from Helium-Backfilled Samples of AA1100 and AA6061 Coupons. *LRS/EXT-21-01823*, **2021**.

(22) G.P. Horne, J.K. Conrad, T.M. Copeland-Johnson, X. Pu, A. Khanolkar, J.R. Wilbanks, and C.D. Pilgrim, Milestone 1.2.10: Steady-state H_2 "roll over" point data for aluminum alloys 1100 and 6061. INL/RPT-22-68379, Revision 0, **2022**.

(23) J.K. Conrad, A.R. Khanolkar, P. Xiaofei, T.M. Copeland-Johnson, C.D. Pilgrim, J.R. Wilbanks, E.H. Parker-Quaife, and G.P. Horne, Radiolytic Gas Production from Aluminium Coupons (Alloy 1100 and 6061) in Helium Environments – Assessing the Extended Storage of Aluminium Clad Spent Nuclear Fuel. *MDPI materials*, **2022**, *accepted*.

(24) T.E. Lister, Vapor Phase Corrosion Testing of Pretreated Al1100. *INL/EXT-18-52249*, **2018**.

(25) A. Abboud, Modeling Summary of ASNF in DOE Sealed Standard Canisters. *INL EXT-21-64413*, **2021**.

(26) A. Abboud, Modeling of Radiolytic Hydrogen Generation of Irradiated Surrogate Aluminum Plates. *INL-RPT-21-66504*, **2021**.

(27) A. Abboud, Extended Modeling of DOE Sealed Canisters with Updated Chemistry Models. *INL-RPT-22-67694*, **2022**.

(28) A.W. Abboud, Sensitivity study of coupled chemical-CFD simulations for analyzing aluminum-clad spent nuclear fuel storage in sealed canisters. *Nuclear Engineering and Design*, **2022**, *390*, 111691.

(29) P. Winston, S. Middlemas, A. Winston, J. Aguiar, X. Liu, and K. Tolman, Aluminum Spent Fuel Performance in Dry Storage Task 4 Aluminum Oxide Sampling of ATR Dry-Stored Fuel. . *INL/EXT-20-58404*, **2020**.

(30) C. Vargel, Corrosion of Aluminium. Elsevier, Amsterdam, **2004**.

(31) D.L. Fisher, M.L. Westbrook, and R.L. Sindelar, Test Results from Gamma Irradiation of Aluminum Oxyhydroxides. *SRNL-STI-2011-00602*, **2012**.

(32) M.L. Westbrook, R.L. Sindelar, and D.L. Fisher, Radiolytic hydrogen generation from aluminum oxyhydroxide solids: theory and experiment. *J. Radioanal. Nucl. Chem.*, **2015**, *303*, 81.

(33) J.A. Kaddissy, S. Esnouf, D. Durand, D. Saffré, E. Foy, and J.-P. Renault, Radiolytic events in nanostructured aluminum hydroxides. *J. Phys. Chem. C*, **2017**, *121*, 6365.

(34) Huestis, P.; Pearce, C.I.; Zhang, X.; N'Diaye, A.T.; Rosso, K.M.; LaVerne, J.A., Radiolytic Stability of Gibbsite and Boehmite with Adsorbed Water, *J. Nucl. Mater.*, **2018**, *501*, 224.

(35) J.A. LaVerne and P.L. Huestis, H atom production and reaction in the gamma radiolysis of thermally modified boehmite. *J. Phys. Chem. C*, **2019**, *123 (34)*, 21005.

(36) C. Verst, A. d'Entremont, B. Radnall, J. McNamara, J. Jarrell, and R. Sindelar, Interim Irradiation and Measurement of As-Dried vs As-Corroded Hydrated Oxide Specimens (Large Coupons). *SRNL-L6000-2021-00006,* **2021**.

(37) J. Perry, R. Demuth, N. Cooper, T. Knight, N. Parisi and G. Stafford; A.W. Abboud, and R.E. Smith, Engineering-Scale Drying of Aluminum-Clad Spent Nuclear Fuel, *INL/EXT 21 62416*, **2021**.

(38) C. Verst, MINI-CANISTER RADIOLYSIS RESULTS – PRELIMINARY RESULTS OF ALTERNATE DRYING RECIPE. *SRNL-L3110-2022-00004*, **2022**.

(39) H. Fricke and E.J. Hart, The Oxidation of Fe^{2+} to Fe^{3+} by the Irradiation with *X*-Rays of Solutions of Ferrous Sulfate in Sulfuric Acid. *J. Chem. Phys.*, **1935**, *3*, 60.

(40) J.W.T. Spinks and R.J. Woods, An Introduction to Radiation Chemistry, Third Edition, Spinks J.W.T.; Woods, R.J. Eds.; Wiley-Interscience, New York, USA, **1990**.

(41) L. Lundberg, Corrosion of Spent ATR Fuel Elements Relative to Their Dry Storage. ERA-NRE-94-096, **1994**.

(42) Glazoff, M.V., Lister, T.E., 2018. Transition of Spent Nuclear Fuel to Dry Storage, INL/EXT-18-51694, **2018**.